Thermochimica Acta, 123 (1988) 73–83
Elsevier Science Publishers B.V., Amsterdam – Printed in The Netherlands

HEAT CAPACITY MEASUREMENTS UNDER HIGH PRESSURE*,**

OSAMU YAMAMURO, MASAHARU OGUNI, TAKASUKE MATSUO and HIROSHI SUGA

Department of Chemistry and Chemical Thermodynamics Laboratory, Faculty of Science, Osaka University, Toyonaka, Osaka 560 (Japan)

(Received 29 January 1987)

ABSTRACT

Heat capacities of hexagonal ice Ih, cubic ice Ic, and Ar gas hydrate were measured by using a newly developed constant high-pressure adiabatic calorimeter. The pressure dependence of the transition temperature of ice XI–Ih was determined and the glass transitional behaviour of ice Ic was observed for the first time. The rattling motion of argon molecules enclathrated in the gas hydrate $Ar \cdot 5.67H_2O$ was analysed from the heat capacity data.

INTRODUCTION

The measurement of heat capacity at different constant pressures is very important, ranking with volume vs. pressure measurements at various constant temperatures, because the Gibbs energy surface can be experimentally obtained from these measurements. Under normal pressures the adiabatic calorimeter is widely used as the most reliable method of obtaining accurate heat capacity values. However, the extension of this method to high pressures is not straightforward owing to many experimental difficulties. The clamp-bomb adiabatic calorimeter generally used cannot work under constant pressure owing to the volume change of substances in the calorimeter cell, and hence is unsuitable for the study of phenomena which have large volume changes (e.g., phase transitions).

We have constructed a new type of adiabatic calorimeter workable under constant high pressures up to 250 MPa. The pressure is automatically controlled within ± 1 kPa by connecting the cell to an external pressure control system through a pressure-transmitting tube. Helium gas, which is chemically inert and does not solidify even at very low temperatures, was used as the pressure-transmitting medium, and enabled us to measure the

* Paper presented at the Sino-Japanese Joint Symposium on Calorimetry and Thermal Analysis, Hangzhou, People's Republic of China, 5–7 November 1986.
** Contribution No. 121 from Chemical Thermodynamics Laboratory.

0040-6031/88/$03.50

heat capacity of almost all solid samples in the wide temperature region 12–400 K. This lower temperature limit is low enough to obtain the third law entropy by extrapolating heat capacity curves down to zero Kelvin.

This calorimeter was applied to the following three hydrogen-bonded systems. (1) The XI–Ih phase transition at 72 K in ice doped with KOH was measured at two pressures (0 and 158.9 MPa), and its pressure dependence and volume change were determined. (2) In the metastable cubic ice Ic formed along the path on the p–T phase diagram (water → III → IX → Ic), a novel glass transition associated with disordered proton configurational motion was found at 140 K. (3) Ar gas-hydrate was synthesized from water and 200 MPa Ar-gas directly in the calorimeter cell, and the motion of guest Ar atoms in the clathrate cage was analyzed from its heat capacity contribution.

APPARATUS

Cryostat

Figure 1 is a schematic drawing of the cryostat of the calorimeter. The greatest difference from previous calorimeters is that the pressure-transmit-

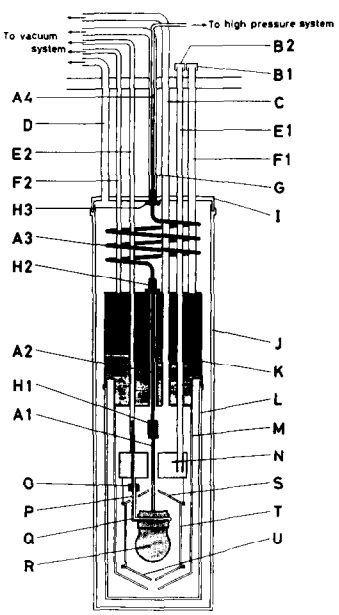

Fig. 1. Schematic drawing of a cryostat. A, high-pressure transmitting tubes; B, caps; C, D, G, pumping tubes; E, liquid nitrogen inlet and outlet; F, liquid hydrogen inlet and outlet; H, couplings; I, J, outer vacuum jacket; M, outer adiabatic shield; N, liquid nitrogen tank; O, joint; P, transfer tube; Q, cooling ring; R, cell; S, T, U, inner adiabatic shields.

ting tubes A1–A4, made of stainless steel, enter the calorimeter cell R from the external high-pressure system. Helium gas, as the pressure-transmitting medium, flows into or out of the cell through these tubes and maintains the pressure inside the cell at a constant value. The tube just above the cell A1 and consequently the helium gas it contains are maintained at the same temperature as the cell.

The calorimeter cell R, whose internal volume is 26 cm^3 and whose mass is 600 g, is made of Cu–Be alloy which has high thermal conductivity and sufficient mechanical strength to withstand the applied pressure. Pressure sealing is established by a metallic cone connection instead of the traditional Bridgman method. The maximum pressure without leaking is about 250 MPa. The nearly spherical shape of the cell was devised in order to minimize the mass and maximize the inside volume. This design helps to increase the ratio of the sample heat capacity to the total capacity and contributes to improvement in precision. The cell is dismountable at the coupling H1.

Temperatures as low as 12 K can be obtained by standard cryogenic techniques using H_2 and N_2 liquids. Normally the cell is cooled with heat-conducting He gas introduced into the jackets J and L. If the sample is volatile, however, it is possible to cool only the cell, leaving the tubes A2–A4 at higher temperatures than the cell, by introducing liquid N_2 directly into the cooling ring Q through E1, N, and P. This ring can be removed at the joint K for measurements of non-volatile samples.

Adiabatic conditions are achieved by the orthodox method: evacuating the space inside the jackets J and L to 10^{-4} Pa and automatically controlling the inner adiabatic shields S, T, U, pressure-transmitting tube A1, and liquid N_2 transfer tube P at the same temperature as the cell.

Calorimetric and high pressure systems

Figure 2 gives the block diagram of calorimetric and high-pressure systems. Calorimetric measurement is carried out in the standard fashion. Temperature is determined by measuring the resistance of the platinum thermometer (470 Ω at 273 K, Minco Products, U.S.A.) installed on the cell H. The automatic a.c. resistance bridge K (ASL F17A, U.K.) gives a ratio of the resistance of the thermometer to that of a standard resistor as a digital output with eight digits. This resistance readout is converted to the temperature using the function of IPTS-68 calibrated in advance. The supplied energy is determined by using the digital multimeter (Keithley 195, U.S.A.) in the energy-supplying circuit M and the digital clock in the microcomputer L (Sharp MZ2200, Japan).

All the measurements, the calculation to find the molar heat capacity of the sample, and the data storage are fully automated functions of the microcomputer L [1]. The use of the computer not only saves labour but also improves the precision of the thermometry. Usually the temperature is read

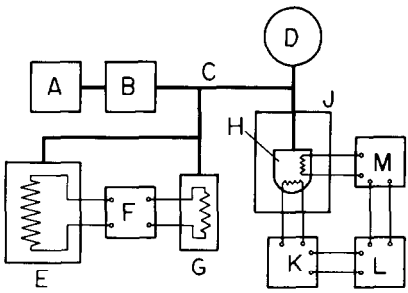

Fig. 2. Block diagram of the calorimetric and high pressure systems. A, helium tank; B, diaphragm compressor; C, high-pressure transmitting tubes; D, Heise gauge; E, helium gas reservoir; F, pressure control circuit; G, manganin wire resistance gauge vessel; H, cell; J, cryostat; K, a.c. resistance bridge; L, computer; M, energy supplying circuit.

out once every 60 s by averaging 12 measurements stored at intervals of 5 s: this procedure greatly reduces the scatter of the data. The precision of the present thermometry is estimated to be within 50 μK at temperatures above 50 K.

High pressure is generated by compressing helium gas supplied from the tank A with the double-headed diaphragm compressor B (NOVA SWISS 554. 3330-2). The pressure is read from the Heise gauge D, whose precision is within $\pm$ 0.1 MPa. The pressure in the cell H is controlled by adjusting the temperature of the helium gas in the reservoir E. Pressure change in the cell is detected as the change in resistance of a manganin wire in the vessel G. The wire constitutes one arm of the Wheatstone bridge in the pressure-regulating circuit F and its deviation from the preset value corresponding to the desired pressure is converted to an electric signal. This signal is amplified with the PID circuit in F and utilized as the current passing through the heater wire in E. The reservoir E is about eight times larger (ca. 200 cm^3) than the cell H and can change its temperature from about 100 °C to 10 °C. This is sufficient to compensate for the pressure increase due to the temperature rise of the cell during a calorimetric measurement (12–400 K). The precision of pressure control is within 1 kPa over the whole pressure and temperature ranges.

This method of pressure control is basically the same as that of the high-pressure calorimeter with a liquid pressure-transmitting medium reported earlier [2]. The precision of pressure control was, however, greatly improved. This was necessary because of changing the pressure-transmitting medium to helium gas which has much larger thermal expansivity (i.e., large heat of compression) than the liquid. Temperature change due to the fluctuation of the pressure of 1 kPa was confirmed to correspond to 15 μK at about 50 K, which is adequately small compared with the precision of the thermometry, i.e. 50 μK.

Adiabatic high-pressure calorimetry suffers the inevitable disadvantage that the heat capacity of the empty cell is much larger than that of the sample. In the present calorimeter the value at 300 K is about 300 J K^{-1} which is ten times larger than that of a typical sample. Considering that heat capacities of the empty cell and the sample are generally comparable in magnitude in the conventional adiabatic calorimeter, the precision of the heat capacity obtained in our calorimeter might have become ten times poorer than that of the ordinary calorimeter (i.e., below 1%). However the actual precision estimated from the test measurement on helium gas at 160 MPa was better than 0.5% over the whole temperature range. This is attributed to the improved thermometry and precise pressure control described above.

EXPERIMENTAL RESULTS

Hexagonal ice

Ordinary ice Ih has positional disorder of protons in the hydrogen-bonded network and a residual entropy of 3.4 J K^{-1} mol^{-1} [3]. In pure ice, we cannot observe the ordering transition for kinetic reasons; i.e., the proton configurational motion is frozen-in at 110 K [4] before the transition takes place on cooling. However an ice specimen doped with a small amount of KOH undergoes a first-order transition at 72 K [5]. This is the intrinsic ordering transition of ice Ih induced by the catalytic action of KOH, which increases the mobility of the protons by creating ionized vertex with an orientational defect. The ordered phase was confirmed to be orthorhombic ($Cmc2_1$) by neutron diffraction measurements of D_2O ice [6] and designated as ice XI [7].

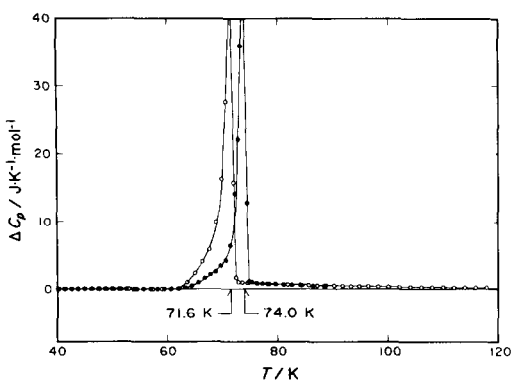

Fig. 3. Excess heat capacity on XI–Ih phase transition. ○, 0 MPa; ●, 158.9 MPa.

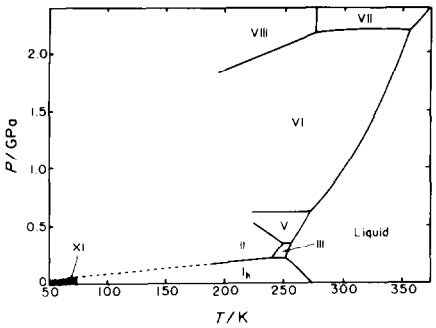

Fig. 4. $p-T$ phase diagram of H_2O.

For the purpose of clarifying the pressure dependence of the XI–Ih transition, we measured the heat capacities of ice Ih doped with KOH ($x = 1.3 \times 10^{-3}$) at two pressures; 0 and 158.9 MPa. In both series the sample was annealed at 65 K for 3 days before the heat capacity measurements because it is known that the Ih–XI transition proceeds slowly and the amount of the ordered phase XI depends on the annealing period. The temperature increment used in the measurement was 0.1 K around the transition point so as to determine the transition temperature precisely.

Figure 3 shows the excess heat capacity associated with the XI–Ih phase transition at two pressures; 0 and 158.9 MPa. A sharp first-order transition was observed at (71.6 ± 0.1) K for 0 MPa and (74.0 ± 0.1) K for 158.9 MPa. Both the peaks had short tails over about 10 K on the low temperature side and long tails over about 50 K on the high temperature side. This is one of the characteristic features of the transition. The pressure dependence of the transition temperature was calculated to be (0.015 ± 0.001) K MPa^{-1} assuming it to be linear. With this value and the residual entropy of 3.4 J K^{-1} mol^{-1}, the use of the Clausius–Clapeyron equation gives the volume changes at the transition as 0.051 ± 0.003 cm^3 mol^{-1}. This value corresponds to 0.26% of the total volume.

Figure 4 shows the $p-T$ phase diagram of H_2O ice. A new phase boundary XI–Ih can be added in the figure obtained by the present direct method. This almost vertical line reflects the negligibly small volume change associated with the proton ordering as observed also in the ice VIII–VII transition.

Cubic ice

Cubic ice Ic with the diamond structure is structurally similar to Ih, with an almost identical arrangement of nearest neighbours, and by reason of symmetry is fully disordered with respect to the positions of protons in the hydrogen-bonded network. This disorder is expected to be frozen-in below

150 K as judged from the dielectric data [8], as for hexagonal ice. However, previous heat capacity measurements on a sample prepared from amorphous ice [9] showed neither phase transition nor glass transition in this temperature range.

We remeasured the heat capacity of cubic ice with the adiabatic high-pressure calorimeter. The cubic ice was prepared in one mole quantity in the calorimeter cell with the following procedure. At first high-pressure ice III was obtained by cooling liquid water under 250 MPa. Next the ice III was cooled down to 80 K through the III–IX transition and the pressure was then released. The ice IX stayed in the metastable state at that temperature, but began to transform to Ic at around 140 K on warming. It took about 7 h for the complete conversion. The measurement was carried out in the range 13–170 K because an irreversible Ic–Ih transition begins to take place around 170 K.

The heat capacity of cubic ice was almost the same as that of hexagonal ice below 100 K. Above 100 K, however, an interesting difference was observed. Figure 5 shows the spontaneous temperature drift rates observed at 20 min after each heating period. Circles represent the data of the sample after rapid cooling (0.8 K min^{-1}). An exothermic drift appeared from about 120 K up to 140 K and then an endothermic drift was observed up to 160 K. The corresponding drift rate of the sample annealed at 133 K for 21 h is represented by triangles. There was almost no exothermic region but a greater endothermic effect appeared from 133 K, the temperature at which the sample was annealed. This figure shows the typical dependence of the drift on temperature in the glass transition region [4], that is an enthalpy relaxation from non-equilibrium to the equilibrium state. Figure 6 shows the encraty (C_p–T) plots corresponding to the data in Fig. 5. Crosses represent the data on hexagonal ice for comparison. Each encraty curve has a jump (about 0.5 J K^{-1} mol^{-1} in C_p) around the temperature where the corre-

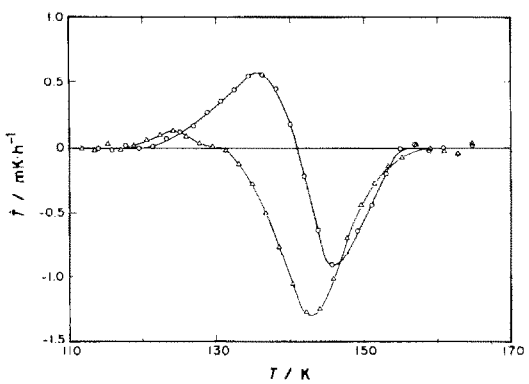

Fig. 5. Spontaneous temperature drift rates in the glass transition region of ice Ic. ○, cooled at 0.8 K min^{-1}; △, annealed at 133 K for 21 h.

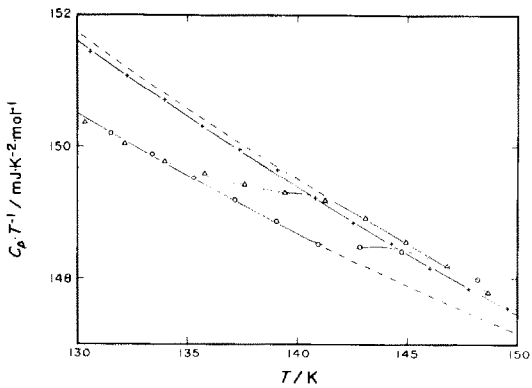

Fig. 6. Encraty (C_p–T) plots in the glass transition region of ice. ○, Ic (cooled at 0.8 K min^{-1}); △, Ic (annealed at 133 K for 2 h); +, Ih (cooled at 0.5 K min^{-1}).

sponding drift rates change its sign from positive to negative. This is because the heat capacity in and below the exothermic region contains no contribution from the mode of molecular motion whose relaxation time is longer than the time scale of the measurement (10^3–10^4 s), while in the higher temperature region the heat capacity is the equilibrium one where all modes are excited. In the present case the mode observed is that of the proton configuration. The broken line on the high temperature side of the glass transition represents the encraty containing no contribution from protons while that on the low temperature side represents a hypothetical equilibrium one from all the modes. The difference between them, corresponding to the configurational heat capacity, increases as the temperature is lowered. This is because the short-range order of the proton configuration is developing with decreasing temperature as observed for hexagonal ice (see previous section).

Thus the glass transition associated with the disordered protons was found at around 140 K which is 30 K higher than that of hexagonal ice at 110 K [4]. At the present moment, however, the hypothetical transition temperature at which long-range proton order would appear in cubic ice is not known. Therefore, doping experiments are being carried out.

Argon gas hydrate

Argon gas hydrate is a cubic crystal belonging to von Stackelberg's structure II [10], whose unit cell contains 16 dodecahedra and 8 hexadecahedra composed of 136 water molecules in total. Argon molecules are enclathrated in cavities of every polyhedron so that the ideal composition is $Ar \cdot 5.67H_2O$. Protons in the host water lattice are expected to be disordered in position and frozen-in above the ordering transition as for ices Ih and Ic. Argon-hydrate is the most fundamental gas hydrate in the sense that Ar is

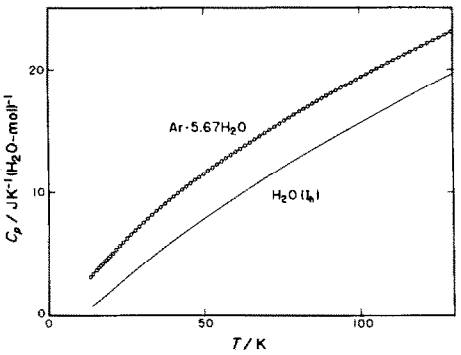

Fig. 7. Heat capacity of $Ar \cdot 5.67H_2O$.

the smallest of the molecules which can be enclathrated in the hydrate lattice and its interaction with the lattice is considered to be the weakest. However, the thermal properties of Ar-hydrate have not been studied so far owing to the difficulties of sample preparation.

The sample of Ar-hydrate was prepared in the calorimeter cell using one mole of water with 200 MPa of Ar gas at around 250 K. Repeated crystallization and melting of water were found to accelerate the formation of the hydrate. The extent of reaction was checked by measuring the enthalpy of fusion of the remaining ice. It took about 50 days to convert 99.7% of H_2O to the hydrate. The crystal was cooled and decompressed carefully so as to avoid decomposition of the hydrate and solidification of Ar gas. Heat capacity measurements were carried out from 15 to 130 K, always keeping the Ar pressure above the decomposition line of the hydrate.

Figure 7 shows the heat capacity of Ar-hydrate represented per mole of H_2O. The lower line shows the molar heat capacity of ice Ih. No anomaly due either to phase transition or glass transition was observed in the whole temperature range. Configurational motion of the protons involved in the hydrogen bonds of the host lattice is believed to be frozen-in before any short-range order develops on cooling.

Assuming that the heat capacity of the host lattice is the same as that of hexagonal ice and that simple additivity of heat capacity is valid, then the contribution from the guest molecules can be separated from the total. The molar heat capacity of Ar enclathrated in the cavities obtained in this way is shown in Fig. 8. The Ar molecule in each cavity undergoes the motion called rattling, which is the motion in limited space and is intermediate in nature between harmonic vibration and free translation. By assuming spherical cages, the potential function relevant to the motion will be reasonably described by the one-dimensional Pöschl–Teller potential

$$V(x) = \frac{h^2 a(a-1)}{8md_0^2 \sin^2[(x/d_0) - 1/2]}$$

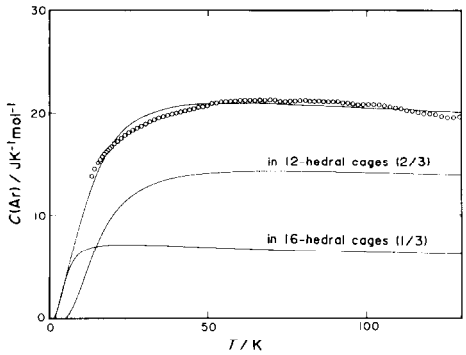

Fig. 8. Molar heat capacity of Ar enclathrated in the cages of the structure II hydrate.

where m is the mass of Ar, d_0 is the diameter of the cavities, and a is a parameter characterizing the stiffness of the walls. The energy levels for this potential are simply

$$E_n = \left(h^2/8md_0^2\right)(a+n)^2 \qquad n = 0, 1, 2\ldots$$

Using this formula for the levels, the least squares fitting was made to reproduce the experimental values of heat capacity. The hydrate has two types of cages (12-hedra and 16-hedra), but only two parameters $a(12)$ and $d_0(12)$ were used by fixing $a(12) = a(16)$ and $d_0(16) - d_0(12) = 160$ pm (actual difference of size of the two cages). The values for the parameters were determined as follows: $a(12) = a(16) = 19$, $d_0(12) = 220$ pm, and $d_0(16) = 380$ pm. The calculated heat capacities reproduce fairly well the experimental ones. This result provides evidence for the validity of the underlying assumptions. On the basis of the present data on Ar-hydrate, we will proceed to calorimetric measurement on other hydrates; e.g., structure I hydrates (Xe, CH_4, etc.) or polar organic molecule hydrates (ethylene oxide, tetrahydrofuran, etc.).

ACKNOWLEDGEMENTS

This work was supported by a Grant-in-Aid for Scientific Research No. 57430002 from the Ministry of Education, Science and Culture. Thanks are extended to many people in the Workshop Center, Osaka University, for their help in designing and constructing the high-pressure calorimeter.

REFERENCES

1 T. Matsuo and H. Suga, Thermochim. Acta, 88 (1985) 149.
2 M. Oguni, T. Watanabe, T. Matsuo, H. Suga and S. Seki, Bull. Chem. Soc. Jpn., 55 (1982) 77.

3 W.F. Giauque and J.W. Stout, J. Am. Chem. Soc., 58 (1936) 1144.
4 O. Haida, T. Matsuo, H. Suga and S. Seki, J. Chem. Thermodyn., 6 (1974) 815.
5 Y. Tajima, T. Matsuo and H. Suga, J. Phys. Chem. Solids, 45 (1984) 1135.
6 A.J. Leadbetter, R.C. Ward, J.W. Clark, P.A. Tucker, T. Matsuo and H. Suga, J. Chem. Phys., 82 (1985) 424.
7 T. Matsuo, Y. Tajima and H. Suga, J. Phys. Chem. Solids, 47 (1986) 165.
8 S.R. Gough and D.W. Davidson, J. Chem. Phys., 52 (1970) 5442.
9 M. Sugisaki, H. Suga and S. Seki, Bull. Chem. Soc. Jpn., 41 (1968) 2591.
10 D.W. Davidson, S.K. Garg, S.R. Gough, Y.P. Handa, C.I. Ratcliffe, J.S. Tse and J.A. Ripmeester, J. Inclusion Phenom., 2 (1984) 231.